RESEARCH ARTICLE

INTERNATIONAL RESEARCH JOURNAL OF MULTIDISCIPLINARY TECHNOVATION

Asian Research Association

DOI: 10.54392/irjmt26427

# Natural Fruit-Juice-Assisted Synthesis of MgO Nanoparticles: Evaluation of Structural, Optical, Vibrational, Thermal, Morphological, and Antimicrobial Properties

**N. Backiyalakshmi [a, *], S. Sindhu Kavi [b], R. Manoranjitham [a], A. Ramalingam [c, *]**

[a] Department of Science and Humanities, KGiSL Institute of Technology, Coimbatore-641035, Tamil Nadu, India
[b] Department of Physics, KPR Institute of Engineering and Technology, Coimbatore-641407, Tamil Nadu, India
[c] Department of Physics, Government Arts College, Udumalpet-642126, Tamil Nadu, India
* Corresponding Authors Email: priasumi@gmail.com ramligri75@gmail.com

DOI: https://doi.org/10.54392/irjmt26427
Received: 09-04-2026; Revised: 08-07-2026; Accepted: 20-07-2026; Published: 30-07-2026

**Abstract:** Magnesium oxide (MgO) nanoparticles have attracted considerable attention because of their distinctive physicochemical properties and their potential biomedical and environmental applications. In this study, grape extract was used as a green fuel and stabilising medium for the synthesis of MgO nanoparticles, thereby avoiding the use of toxic chemicals. The effects of post-synthesis annealing at two temperatures on the structural, morphological, optical, and thermal properties of the nanoparticles were investigated. Crystalline MgO nanoparticles were confirmed by powder X-ray diffraction (PXRD), Fourier-transform infrared spectroscopy (FTIR), UV-visible spectroscopy, zeta-potential analysis, and electron microscopy. The calculated crystallite sizes were 7.21 nm for MgO, 7.24 nm for MgO-350, and 8.43 nm for MgO-450. Increasing the annealing temperature improved crystallinity and lattice ordering, reduced surface defects, and influenced particle size and optical band-gap behaviour. The synthesised MgO nanoparticles also exhibited antimicrobial activity against the tested bacterial strains, which may be associated with reactive oxygen species, surface-defect sites, and strong interactions between the nanoparticles and microbial cell membranes. Green-synthesised MgO nanoparticles prepared under optimised annealing conditions therefore show promise for antimicrobial and biomedical applications.

**Keywords:** Green Synthesis, MgO Nanoparticles, Thermal Annealing, Antimicrobial Properties.

## 1. Introduction

Nanotechnology has become an important field within advanced materials science because it enables the development of nanoscale materials with distinctive physicochemical and biological properties. Among the various classes of nanomaterials, metal-oxide nanoparticles have attracted substantial attention because of their high surface-area-to-volume ratio, tunable morphology, enhanced reactivity, and improved catalytic and antimicrobial performance [1, 2]. Magnesium oxide (MgO) nanoparticles are particularly significant because of their excellent thermal stability, high surface energy, biocompatibility, and relatively low toxicity compared with many other metal-oxide nanomaterials. These characteristics make MgO nanoparticles promising candidates for environmental remediation, catalysis, sensors, biomedical devices, and antimicrobial coatings [2-5].

Conventional routes for synthesising MgO nanoparticles include sol-gel processing, co-precipitation, hydrothermal or solvothermal synthesis, solution combustion, and thermal decomposition [1, 3, 6]. Although these methods can produce nanoparticles with controlled morphology and crystallinity, they often require toxic reagents, high temperatures, and complex processing conditions. These limitations have encouraged the development of environmentally friendly alternatives. Green synthesis has therefore emerged as a sustainable approach in which biological resources, including plant extracts, microorganisms, and biomolecules, function as reducing, capping, and stabilising agents, thereby reducing the need for hazardous reagents and harsh reaction conditions [2, 7].

Plant-mediated synthesis is of considerable interest because plant extracts contain a wide range of bioactive molecules, including phenolics, alkaloids, flavonoids, proteins, terpenoids, and polysaccharides. These molecules can act as stabilising, capping, and reducing agents during nanoparticle formation [8, 9]. By regulating nucleation and particle growth and contributing to metal-ion conversion, these biomolecules

can facilitate the formation of stable nanostructures with enhanced biological activity. Plant-based synthesis is also simple, cost-effective, scalable, environmentally benign, and biocompatible, making it suitable for the large-scale production of nanoparticles.

Recent years have seen a surge in interest in the synthesis of magnesium oxide nanoparticles (MgO NPs) using environmentally benign resources such as plant extracts and fruit juices, primarily because of the improved biological characteristics and environmentally friendly production routes [10-19]. Tannins, flavonoids, alkaloids, glycosides, and saponins are bioactive substances present in plant-derived synthesis media and can contribute bactericidal and bacteriostatic effects [8, 9]. Muhaymin et al. synthesised MgO NPs using Hyphaene thebaica plant extract and studied their photocatalytic activity [10]. Lithi *et al.* reviewed plant-extract-mediated green synthesis for antimicrobial applications [2]. Several plant species, including Lawsonia inermis [12], Moringa oleifera [13], Citrus limon [15], Hibiscus rosa-sinensis [16], and Bauhinia variegata [17], have been used for the biosynthesis of MgO nanoparticles. Green-synthesised MgO nanoparticles have demonstrated antimicrobial activity against microorganisms including Escherichia coli, Staphylococcus aureus, Bacillus subtilis, and Pseudomonas aeruginosa [12, 14, 17]. Thamizharasan *et al.* highlighted the antibacterial activity of plant-mediated MgO nanoparticles against dental pathogens and their potential use in oral healthcare and antimicrobial coatings [18]. Coelho et al. demonstrated the role of MgO in a hydroxyapatite bone substitute [5], while Pugazhendhi et al. reported antimicrobial and anticancer effects of green-synthesised MgO NPs [19].

The antimicrobial activity of MgO NPs is associated with several mechanisms, including reactive oxygen species (ROS) production, disruption of bacterial cell membranes, and the release of $Mg^{2+}$ ions that interfere with cellular metabolic processes [17, 20]. In addition, the alkaline nature of MgO nanoparticles can produce a bactericidal effect by altering local pH conditions and damaging cellular structures [4, 5]. The antimicrobial efficiency of MgO nanoparticles is strongly influenced by particle size, morphology, surface charge, and synthesis method [17, 20]. Green synthesis can produce nanoparticles with relatively clean, phytochemical-functionalised surfaces, enhancing their interaction with microbial cells and improving antimicrobial performance [2, 7, 8]. Consequently, plant-mediated MgO nanoparticles are being explored for applications including antibacterial agents, water purification systems, food-packaging materials, biomedical coatings, and antifungal surfaces [18, 19, 22].

Despite growing interest in the green synthesis of MgO nanoparticles, further studies are required to optimise synthesis parameters, clarify antimicrobial mechanisms, and evaluate cytotoxicity and environmental safety [1, 2, 7]. Selection of suitable plant sources and control of nanoparticle morphology also remain important challenges for reproducible and scalable production [1, 8, 23]. Addressing these challenges will support the development of sustainable nanomaterials with improved antimicrobial performance.

The present study focuses on the green synthesis of MgO nanoparticles using grape extract as a fuel, reducing medium, and stabilising agent, and on the influence of annealing temperature on the physicochemical properties of the synthesised MgO nanoparticles. This environmentally friendly approach provides a sustainable route for nanoparticle synthesis and allows the phase purity and crystallinity of MgO to be controlled through annealing. The resulting materials may also support the development of effective antimicrobial systems for addressing microbial contamination and the growing challenge of antibiotic resistance.

## 2. Materials and Methods

### 2.1 Chemical reagents

All chemicals used in this study were of analytical grade and were used without further purification. Magnesium nitrate hexahydrate ($Mg(NO_3)_2{\cdot}6H_2O$, ≥98% purity) was purchased from Merck, India. Distilled water was used as the solvent throughout the synthesis procedure.

### 2.2 Extraction of Vitis Vinifera Fruits

Fresh, commercially purchased Vitis vinifera (grape) fruits were washed thoroughly and crushed using a mortar and pestle. The fruit pulp was removed with a strainer, and the resulting extract was further filtered through filter paper. The filtrate was then centrifuged to remove fine suspended solids. The pH of the fresh grape extract was 5.4, indicating an acidic medium attributable to the organic compounds present in the extract.

### 2.3 Solution-Combustion Synthesis of MgO Nanoparticles

MgO nanoparticles were prepared by grape-extract-assisted solution combustion synthesis. The Vitis vinifera extract served as the fuel and provided phytochemicals that assisted the combustion process. To prepare a 1 M precursor solution, 12.82 g of magnesium nitrate hexahydrate ($Mg(NO_3)_2{\cdot}6H_2O$) was dissolved in 50 mL of distilled water. The solution was stirred magnetically for 1 h to ensure complete and uniform dissolution of the magnesium nitrate. Subsequently, 50 mL of grape extract was added slowly to facilitate interactions between $Mg^{2+}$ ions and the

phytochemicals present in the extract. The resulting mixture was stirred for a further 1 h.

The homogeneous solution was then heated on a hot plate at 100 °C. Heating caused solvent evaporation and the formation of a viscous precursor, which subsequently underwent solution combustion with the release of gaseous products, ultimately yielding a solid magnesium oxide product. After completion of the combustion reaction, the MgO solid was ground into a fine powder using an agate mortar and pestle. The powder was then washed and dried through three cycles to remove moisture and unreacted organic species. The overall synthesis procedure is illustrated in Figure 1.

To examine the effect of post-synthesis heat treatment on the physicochemical properties, portions of the as-prepared sample were calcined at 350 °C and 450 °C, respectively. The samples were labelled MgO (as-prepared), MgO-350, and MgO-450.

### 2.4. Characterisation

Crystallinity and phase purity were examined by powder X-ray diffraction (PXRD) using a Bruker D8 diffractometer with Cu Kα radiation (λ = 1.5406 Å), operated at 30 mA and 40 kV. Fourier-transform infrared (FTIR) spectra were recorded using a Thermo Fisher Scientific Nicolet iS5 spectrometer over the range 500-4000 cm−1. Surface morphology and elemental composition were examined using a Carl Zeiss Merlin Compact field-emission scanning electron microscope equipped with energy-dispersive X-ray spectroscopy. Zeta potential was measured using an Anton Paar Litesizer 500 particle-size analyser. Optical properties were studied using a JASCO V-770 UV-visible spectrophotometer. Thermal behaviour was evaluated using a PerkinElmer thermogravimetric analyser under nitrogen flow at a heating rate of 15 °C $min^{-1}$ over the temperature range 30-900 °C.

## 3. Results and Discussion

MgO nanoparticles were successfully synthesised using plant extract through a solution combustion method. The functional groups and bonding in the synthesised nanoparticles were analysed using Fourier-transform infrared (FTIR) spectroscopy. The FTIR spectrum in Figure 2 shows a strong absorption band centred at approximately 516 $cm^{-1}$, corresponding to Mg-O stretching vibrations characteristic of the MgO lattice and confirming MgO formation [10]. The band width can be ascribed to the nanoscale dimensions of the particles. Weak bands below 500 $cm^{-1}$ are associated with Mg-O lattice vibrations, and the peak at 859 $cm^{-1}$ is associated with Mg-O stretching [21]. Bands between approximately 1129 and 1700 $cm^{-1}$ are assigned to C-O stretching and C-H bending vibrations and may arise from residual organic species or stabilising biomolecules. The band at approximately 1630 $cm^{-1}$ is attributed to bending vibrations of adsorbed water molecules, while peaks near 1400 $cm^{-1}$ indicate carbonate groups caused by atmospheric $CO_2$ adsorption. The peak at approximately 2960 $cm^{-1}$ corresponds to C-H stretching [10, 21]. The broad band at 3400-3450 $cm^{-1}$ is assigned to O-H stretching of hydroxyl groups and physically adsorbed water molecules.

Crystallinity and crystal structure were investigated using powder X-ray diffraction (PXRD). The XRD peaks in Figure 3 at 2θ values of 38.2°, 42.8°, 62.3°, 74.7°, and 78.6° correspond to the (111), (200), (220), (311), and (222) planes of cubic MgO, respectively (JCPDS Card No. 97-7746) [10]. The intense, sharp peak at 2θ ≈ 42.8° for the (200) plane indicates high crystallinity. Characteristic peak intensity increases with annealing temperature, indicating improved phase purity and crystallinity. The peak corresponding to the (111) plane becomes more prominent at higher annealing temperature, as shown by the shaded region in Figure 3.

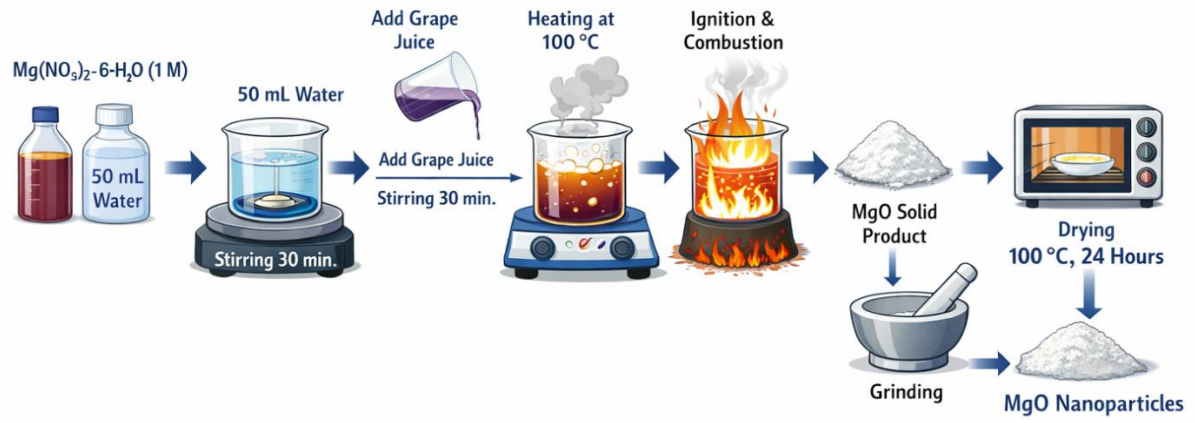


**Figure 1.** Schematic of the synthesis of MgO nanoparticles using grape extract by solution combustion method.

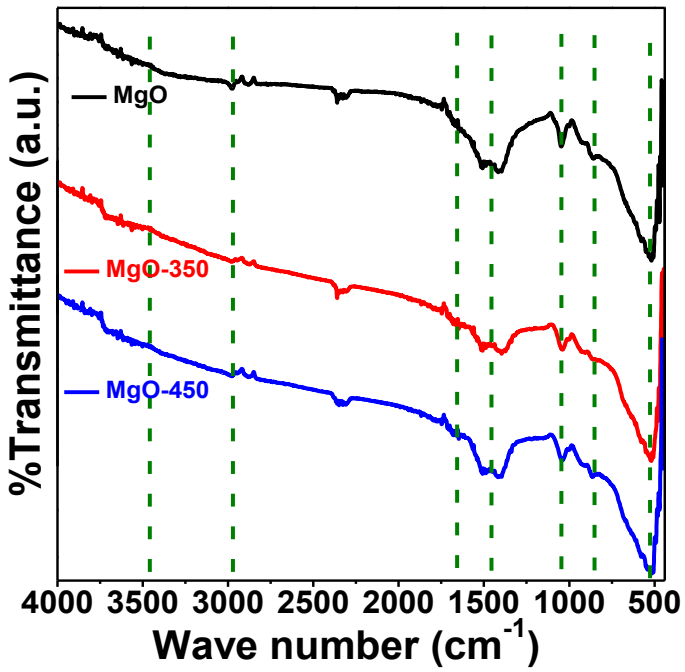


**Figure 2.** FTIR spectra of MgO nanoparticles.

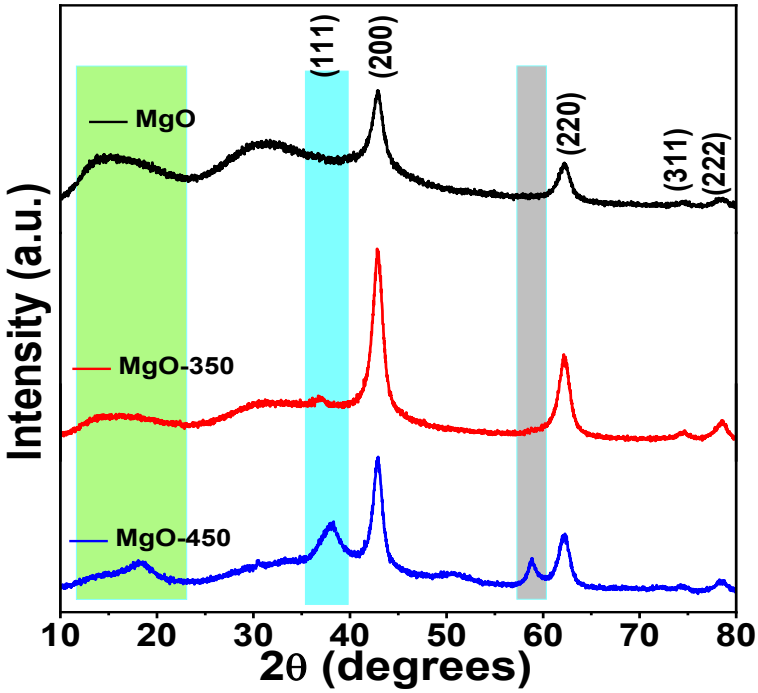


**Figure 3**. XRD patterns of MgO nanoparticles.

The Debye-Scherrer equation was used to calculate the average crystallite size (D) of the nanoparticles:

$$D = \frac{0.94\lambda}{\beta cos\theta} \quad (1)$$

The average crystallite sizes calculated using the Scherrer equation and reported in Table 1 were 7.21, 7.24, and 8.43 nm for MgO, MgO-350, and MgO-450, respectively. The crystallite size of MgO-350 is comparable to that of the as-prepared MgO, indicating that annealing at 350 °C does not cause a substantial change. The increase at 450 °C indicates crystal growth at the higher annealing temperature, consistent with reported calcination-temperature effects on MgO crystallite size [26]. Zeta potential is an important electrokinetic parameter for evaluating nanoparticle surface charge and colloidal stability because it reflects the extent of electrostatic attraction or repulsion between particles in suspension. Measurements were performed in a dispersion medium with a viscosity of 0.895 mPa·s.

The synthesised MgO nanoparticles exhibited slightly negative zeta-potential values, which may be associated with the adsorption of phytochemical constituents from the grape extract onto the nanoparticle surfaces. Functional groups such as carboxylates and phenolates derived from these biomolecules may contribute to the observed negative surface charge. The corresponding zeta-potential distributions are shown in Figure 4a-c. The measured zeta-potential values ranged from -0.1 to -0.6 mV (Table 2), indicating weak electrostatic stabilisation of the nanoparticle suspensions. Although the magnitude of the negative zeta potential increased slightly with annealing temperature, the change was too small to indicate a meaningful improvement in colloidal stability. The conductivity and electrophoretic mobility values of all samples are also presented in Table 2.

Particle morphology was studied using field-emission scanning electron microscopy (FESEM). The FESEM images in Figure 5 show predominantly spherical, agglomerated MgO nanoparticles. The observed morphology supports the role of grape-extract phytochemicals, including polyphenols, flavonoids, and other antioxidant compounds, in controlling nucleation and growth [19]. These bioactive molecules can act as stabilising agents and help limit excessive agglomeration during nanoparticle formation. The plant-derived compounds may also influence the surface energy of growing nuclei and promote comparatively isotropic particle growth [2, 8, 19]. Elemental composition was examined by FESEM-EDX analysis, as shown in Figure 6a-c. The measured Mg:O atomic ratios deviate from the ideal 1:1 stoichiometry, which may result from the semi-quantitative nature of EDX, surface hydroxylation, adsorbed oxygen-containing species, and instrumental limitations.

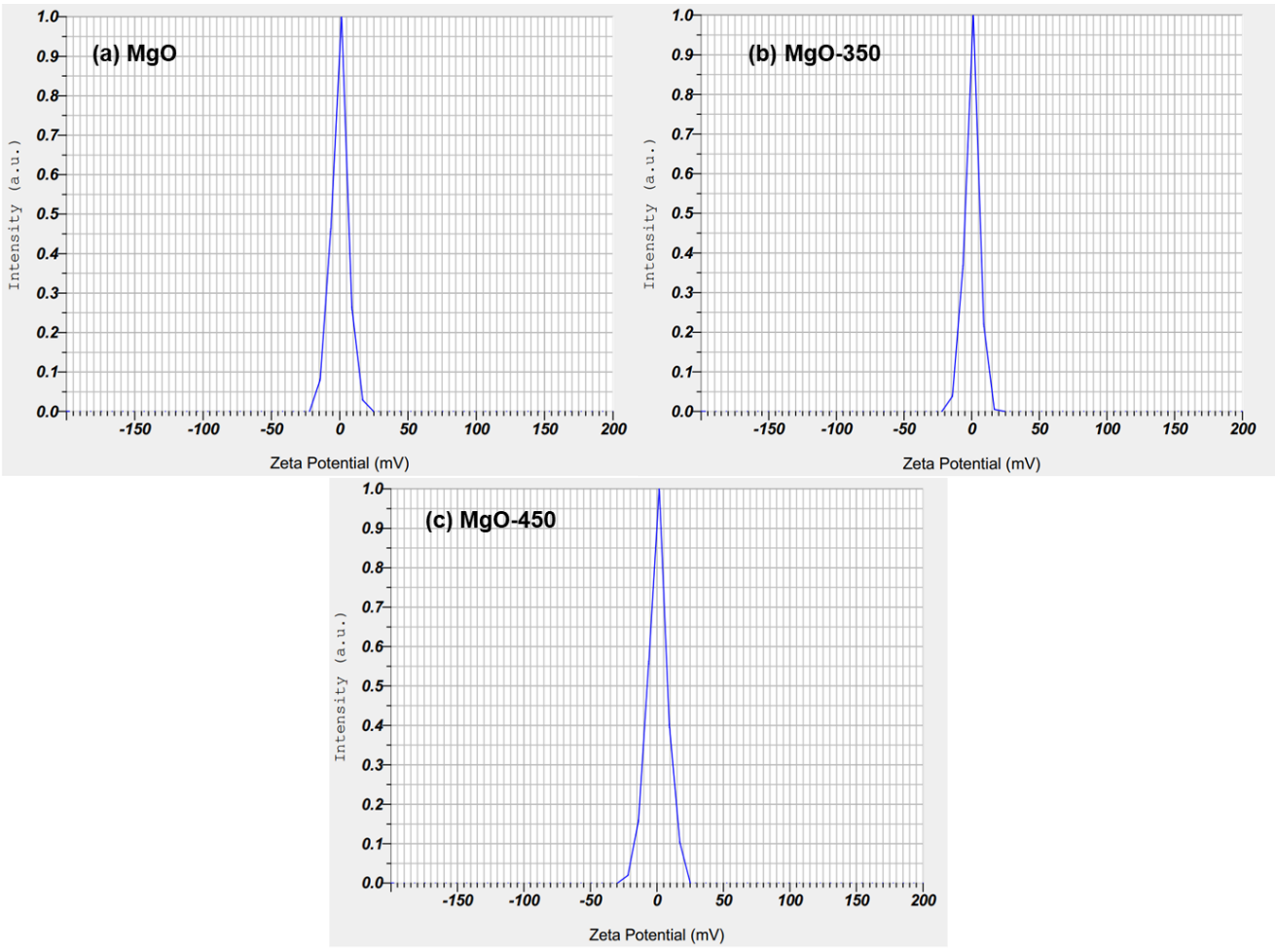


**Figure 4. (a-c)** Zeta-potential distributions of MgO nanoparticles.

**Table 1.** Average crystallite size calculated from XRD data.

| Sample | Avg. crystallite size (D) |
|---|---|
| MgO | 7.21 nm |
| MgO-350 | 7.24 nm |
| MgO-450 | 8.43 nm |

**Table 2.** Zeta potential (mean), conductivity, and electrophoretic mobility of MgO nanoparticles.

| Sample | Zeta potential (mV) | Conductivity (mScm-1) | Electrophoretic mobility ($cm^2V^{-1}s^{-1}$) |
|---|---|---|---|
| MgO | -0.1 | 0.19 | 1×10-6 |
| MgO-350 | -0.2 | 0.08 | 1×10-6 |
| MgO-450 | -0.6 | 0.22 | 3×10-6 |

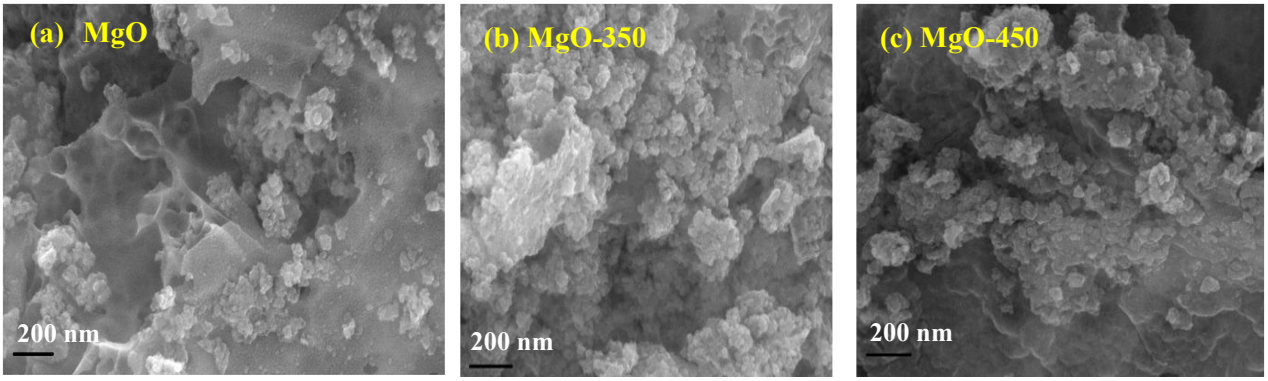


**Figure 5. (a-c)** FESEM images of MgO nanoparticles. The scale bars correspond to 200 nm.

The inset compositions in Figure 6 indicate a modest decrease in the measured oxygen fraction after annealing.

### 3.1 Thermal Analysis

Thermogravimetric analysis (TGA) was used to investigate the thermal characteristics of the MgO nanoparticles. Figure 7 shows a multistep mass-loss pattern from 30 to 900 °C, indicating the removal of surface species and intermediates during heating. Below approximately 150 °C, the initial mass loss is attributed to physically adsorbed water and volatile contaminants. The second stage, between approximately 150 and 350 °C, is attributed to decomposition of organic residues and surface-bound biomolecules introduced by the green synthesis process [24].

A further minor mass loss between 350 and 500 °C may be associated with decomposition of magnesium hydroxide intermediates and removal of strongly bound organic species. Above 600 °C, the curve becomes nearly constant, indicating increased thermal stability of the remaining MgO phase [24-26].

### 3.2 Optical Absorption Characteristics

The green synthesis route introduces bioactive phytochemicals that function as stabilising and reducing agents and can influence the surface electronic states of the nanoparticles. These surface states may contribute additional absorption features in the UV-visible region. Nanoscale dimensions, annealing-induced changes in crystallinity, and defect-related energy levels collectively determine the optical response of the material. Such optical characteristics may be advantageous for photocatalytic and antimicrobial applications, in which light absorption and surface reactivity play important roles.

The optical properties of the green-synthesised MgO nanoparticles were studied using UV-visible diffuse-reflectance spectroscopy (UV-vis DRS). As shown in Figure 8a, the absorption maxima (λmax) of MgO, MgO-350, and MgO-450 were 559, 556, and 445 nm, respectively.The absorption bands observed near 556 nm are more reasonably attributed to defect-related electronic transitions associated with oxygen vacancies and surface states than to the intrinsic band-to-band absorption of MgO [27, 28].

Bulk MgO has a wide band gap of approximately 7.8 eV and therefore absorbs primarily in the deep-ultraviolet region. In nanostructured MgO prepared by green synthesis, oxygen vacancies, surface defects, and impurity states can introduce localised levels within the band gap, allowing sub-band-gap transitions and visible-region absorption [27, 28].

Phytochemicals such as polyphenols, flavonoids, and tannins may also remain adsorbed on the nanoparticle surface and modify its electronic environment [8, 9].

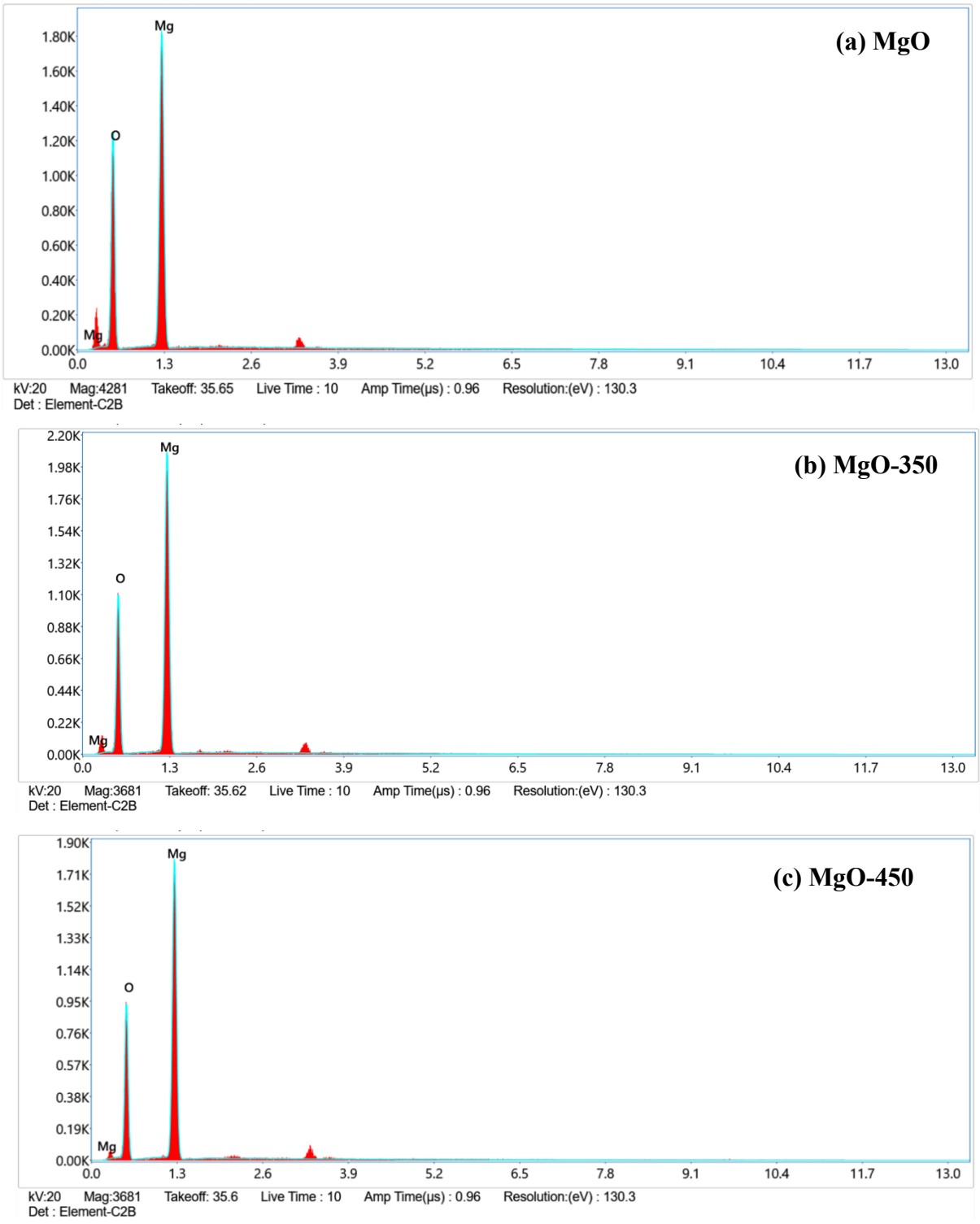


**Figure 6.** EDX analyses of the (a-c) as-prepared and annealed MgO nanoparticles.

Similar defect-induced optical features have been reported for MgO and related metal-oxide nanostructures, where oxygen vacancies and surface states generate colour centres responsible for visible absorption [27, 28]. Therefore, the feature around 445-560 nm is most plausibly associated with defect-related transitions and surface states. The UV-visible absorption spectra show a hypsochromic (blue) shift with increasing annealing temperature, indicating a change in the optical response of the nanoparticles. This shift towards shorter wavelengths may be related to improved crystallinity and a reduction in structural defects during thermal treatment. At higher annealing temperatures, the removal of surface-bound organic residues and volatile impurities can produce a more ordered lattice and reduce defect-related states within the band structure.

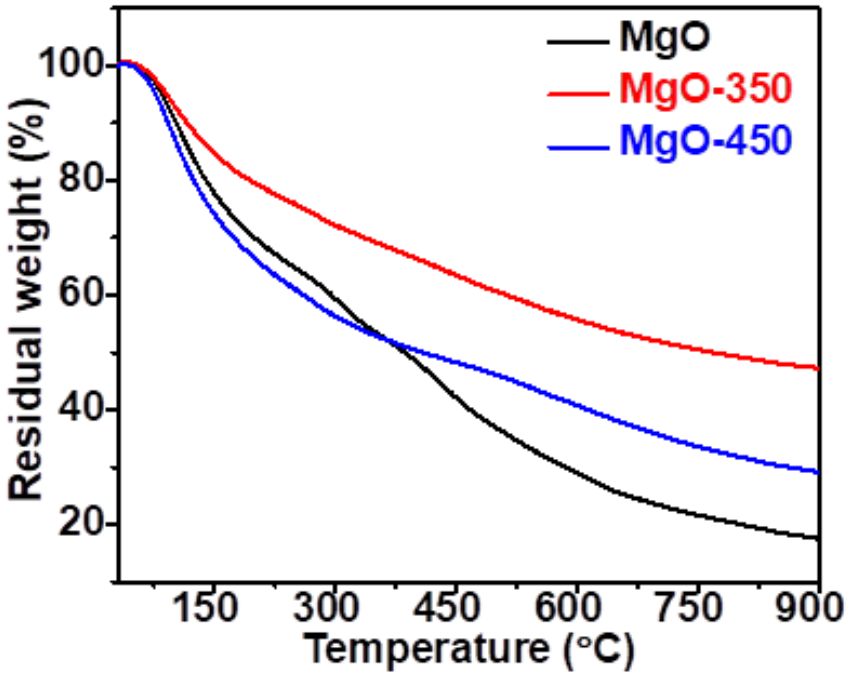


**Figure 7.** TGA curves of MgO nanoparticles.

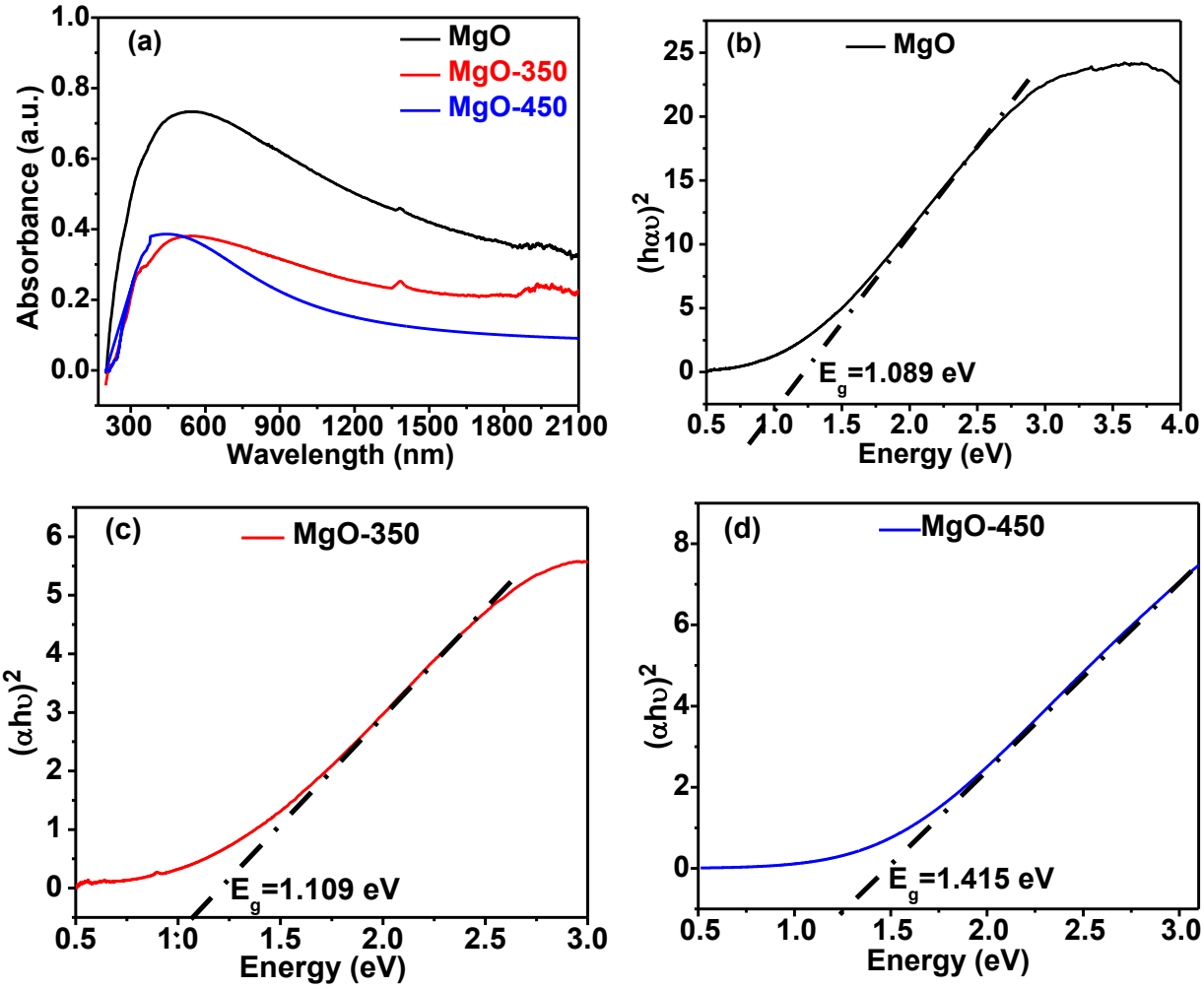


**Figure 8. (a)** UV-vis DRS spectra of the MgO nanoparticles. **(b-d)** Tauc plots used to estimate the optical transition energies of the nanoparticles.

A reduction in oxygen vacancies and trap states may consequently increase the effective optical transition energy, producing a blue shift in the absorption feature. Thermal treatment can also modify the surface electronic environment and influence charge-carrier transitions. Such changes are commonly observed in annealed metal-oxide nanoparticles and are consistent with enhanced structural stability and optical quality.

The reflectance data were converted using the Kubelka-Munk function, and the optical transition energy was estimated from a Tauc plot. The Tauc plots were constructed using the Tauc relation [29] and are shown in Figure 8b-d.

$$(\alpha h\nu)^{1/n} = A(h\nu - E_g) \quad (2)$$

$\alpha\nu E_g$where α is the absorption coefficient, h is Planck's constant, v is the frequency, n = 0.5 was assumed for a direct allowed transition, A is a proportionality constant, and Eg is the optical band gap [29, 30].

The optical transition energy was estimated by extrapolating the selected linear region of the (αhv)2 versus photon-energy (hv) plot to the energy axis. For the present analysis, n = 0.5 was used under the assumption of a direct allowed electronic transition.$(\alpha h\nu)^{1/n}$

Photon energy was calculated using Equation (3).

$$h\nu = \frac{1240}{\lambda\,(nm)}\ \text{eV} \quad (3)$$

The direct-transition values estimated for MgO, MgO-350, and MgO-450 were 1.089, 1.109, and 1.415 eV, respectively. These values are much smaller than the intrinsic band gap of bulk MgO (approximately 7.8 eV) [1, 30]. The discrepancy may reflect defect-related absorption, surface states, and limitations in selecting the linear Tauc region; therefore, these values should not be interpreted uncritically as the intrinsic MgO band gap [27-30].

### 3.3 Antibacterial Activity

The disc-diffusion method was used to evaluate antibacterial activity against two bacterial strains. At a concentration of 1 mg/mL, the measured inhibition varied with annealing temperature. The representative inhibition-zone photographs are shown in Figure 9, and the corresponding quantitative comparison is presented in Figure 10.

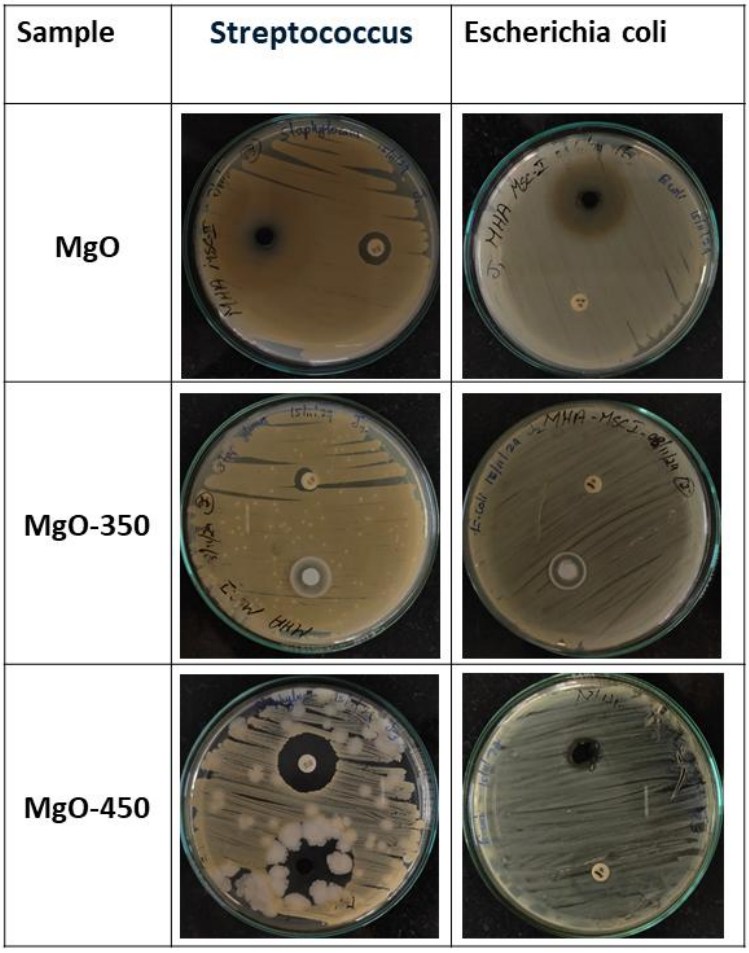


**Figure 9.** Photographs of the inhibition zones produced by MgO nanoparticles.

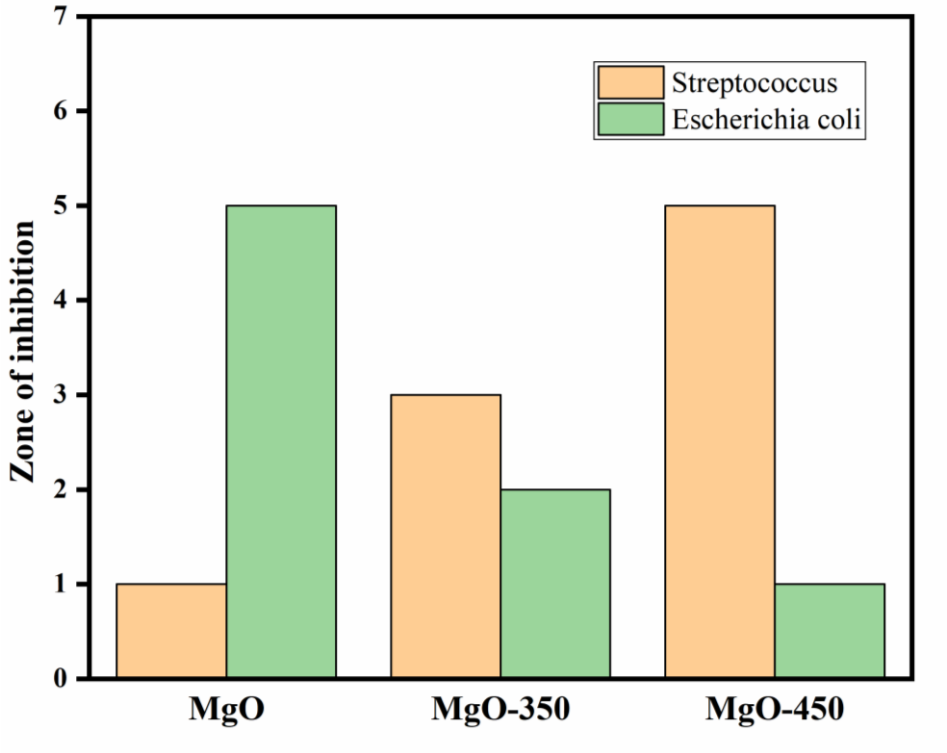


**Figure 10.** Bar-chart comparison of the antibacterial activity of MgO nanoparticles against the two tested bacterial strains.

The as-prepared MgO and MgO-450 samples showed the strongest reported activity against Gram-negative Escherichia coli and Gram-positive Streptococcus, respectively. The antibacterial action of MgO nanoparticles may involve electrostatic interactions with the bacterial surface, followed by the generation of reactive oxygen species such as superoxide anions and hydroxyl radicals. These species can induce oxidative stress, damage cellular components, disrupt membrane integrity, and ultimately cause cell death [20, 4, 31].

## 4. Conclusions

MgO nanoparticles were successfully synthesised through a green solution-combustion route using grape extract. The influence of annealing at 350 °C and 450 °C on the structural, vibrational, morphological, thermal, optical, and antimicrobial properties of the materials was systematically examined. PXRD confirmed the cubic MgO phase, and the calculated crystallite size increased from 7.21 nm for the as-prepared sample to 8.43 nm after annealing at 450 °C, indicating thermally promoted crystal growth. FTIR spectroscopy confirmed Mg-O vibrations and the presence of surface hydroxyl and residual organic groups. FESEM revealed predominantly spherical, agglomerated particles, while EDX confirmed the presence of magnesium and oxygen. The very small negative zeta-potential values indicated weak electrostatic stabilisation of the dispersions. Thermal analysis showed progressive removal of adsorbed water, organic residues, and intermediate species during heating. UV-visible diffuse-reflectance analysis revealed visible-region absorption features that were assigned to defect-related and surface-state transitions; these features shifted towards shorter wavelengths with increasing annealing temperature. The MgO samples also exhibited measurable antibacterial activity against Escherichia coli and Streptococcus, with the response varying according to annealing condition. Overall, grape-extract-assisted combustion provides an environmentally preferable route for producing MgO nanoparticles with tunable physicochemical and antimicrobial properties. Future work should include particle-size distribution analysis, minimum inhibitory concentration measurements, cytotoxicity testing, and mechanistic studies to establish the relationship between annealing, surface defects, and biological performance.

## References

[1] M.A. Gatou, E. Skylla, P. Dourou, N. Pippa, M. Gazouli, N. Lagopati, E.A. Pavlatou, Magnesium Oxide(MgO) Nanoparticles: Synthetic Strategies and Biomedical Applications. Crystals, 14(3), (2024) 215. https://doi.org/10.3390/cryst14030215

[2] I.J. Lithi, K.I.A. Nakib, A.M.S. Chowdhury, M.S. Hossain, A Review on the Green Synthesis of Metal (Ag, Cu, and Au) and Metal Oxide (ZnO, MgO, $Co_3O_4$, and $TiO_2$) Nanoparticles using Plant

Extracts for Developing Antimicrobial Properties. Nanoscale Advances, 7, (2025) 2446–2473. https://doi.org/10.1039/d5na00037h

[3] S.V.G. Kumari, K. Pakshirajan, G. Pugazhenthi, Synthesis and Characterization of MgO Nanostructures: A Comparative Study on the Effect of Preparation Route. Materials Chemistry and Physics, 294, (2023) 127036. https://doi.org/10.1016/j.matchemphys.2022.127036

[4] S. Abinaya, P.K. Helen, Magnesium Oxide Nanoparticles: Effective Antilarvicidal and Antibacterial Agents. ACS Omega, 8(6), (2023) 5225–5233. https://doi.org/10.1021/acsomega.2c01450

[5] C.C. Coelho, T. Padrao, L. Costa, M.T. Pinto, P.C. Costa, V.F. Domingues, P.A. Quadros, F.J. Monteiro, S.R. Sousa, The Antibacterial and Angiogenic Effect of Magnesium Oxide in a Hydroxyapatite Bone Substitute. Scientific Reports, 10(1), (2020) 19098. https://doi.org/10.1038/s41598-020-76063-9

[6] S.K. Alla, A.D. Verma, V. Kumar, R.K. Mandal, I. Sinha, N.K. Prasad, Solvothermal Synthesis of CuO–MgO Nanocomposite Particles and their Catalytic Applications. RSC Advances, 6(66), (2016) 61927–61933. https://doi.org/10.1039/c6ra03762c

[7] D-M. Radulescu, V-A. Surdu, A. Ficai, D. Ficai, A-M. Grumezescu, E. Andronescu, Green Synthesis of Metal and Metal Oxide Nanoparticles: A Review of the Principles and Biomedical Applications. International journal of molecular sciences, 24(20), (2023) 15397. https://doi.org/10.3390/ijms242015397

[8] C. Hano, B.H. Abbasi, Plant-Based Green Synthesis of Nanoparticles: Production, Characterization and Applications. Biomolecules, 12, (2021) 31. https://doi.org/10.3390/biom12010031

[9] S. Iravani, Green Synthesis of Metal Nanoparticles using Plants. Green Chemistry, 13(10), (2011) 2638–2650. https://doi.org/10.1039/c1gc15386b

[10] A. Muhaymin, H.E.A. Mohamed, K. Hkiri, A. Safdar, S. Azizi, M. Maaza, Green Synthesis of Magnesium Oxide Nanoparticles using Hyphaene thebaica Extract And their Photocatalytic Activities. Scientific Reports, 14(1), (2024) 20135. https://doi.org/10.1038/s41598-024-71149-0

[11] A. Sharmila, A. R. Darshan, V. M. Hadkar, N. K. Sishu, C. I. Selvaraj, Green fabrication of Hildegardia populifolia (Roxb.) derived MgO nanoparticles exhibiting potential antioxidant, antibacterial, and photocatalytic properties, Inorganic Chemistry Communications, 172 (2025) 113730. https://doi.org/10.1016/j.inoche.2024.113730

[12] A. Akshaykranth, N. Jayarambabu, V.R. Tumu, R.K. Rajaboina, Comparative Study on Antibacterial Activity of MgO Nanoparticles Synthesized from *Lawsonia Inermis* Leaves Extract and Chemical Methods. Journal of Inorganic and Organometallic Polymers and Materials, 31(6), (2021) 2393–2400. https://doi.org/10.1007/s10904-021-01915-4

[13] S. Vijayakumar, J. Chen, Z.I.G. Sanchez, K. Tungare, M. Bhori, E.F. Durán-Lara, P. Anbu, Moringa Oleifera Gum Capped MgO Nanoparticles: Synthesis, Characterization, Cyto- and Ecotoxicity Assessment. International Journal of Biological Macromolecules, 233, (2023) 123514. https://doi.org/10.1016/j.ijbiomac.2023.123514

[14] R.B. Rotti, D.V. Sunitha, R. Manjunath, A. Roy, S.B. Mayegowda, A.P. Gnanaprakash, S. Alghamdi, M. Almehmadi, O. Abdulaziz, M. Allahyani, A. Aljuaid, A.M. Alsaiari, S.S. Ashgar, A.O. Babalghith, A.E.A. El-Lateef, E.B. Khidir, Green Synthesis of MgO Nanoparticles and its Antibacterial Properties. Frontiers in Chemistry, 11, (2023) 1143614. https://doi.org/10.3389/fchem.2023.1143614

[15] R.V. Poonguzhali, M. Srimathi, E.R. Kumar, N. Arunadevi, H.O. Elansary, A.A. A. Abdelbacki, S.A.M. Abdelmohsen, Citrus Limon Assisted Green Synthesis of MgO Nanoparticles: Evaluation of Phase, Functional Groups, Surface Morphology, Thermal Stability and Colloidal Stability. Ceramics International, 48, (2022) 27774–27778. https://doi.org/10.1016/j.ceramint.2022.06.078

[16] M.A. Khan, F. Ali, S. Faisal, M. Rizwan, Z. Hussain, N. Zaman, Z. Afsheen, M.N. Uddin, N. Bibi, Exploring the therapeutic potential of Hibiscus rosa sinensis synthesized cobalt oxide (Co3O4-NPs) and magnesium oxide nanoparticles (MgO-NPs). Saudi Journal of Biological Sciences, 28(9), (2021) 5157-5167. https://doi.org/10.1016/j.sjbs.2021.05.035

[17] F. Aziz, A.B. Gulshan, Z. Usman, M. Rehman, Q. Khalid, M.N. Khan, M.U. Munir, H.T. Masood, M. Rafique, Facile Eco-Friendly Synthesis of Magnesium Oxide Nanocarriers using Bauhinia Variegata For Biomedical And Photocatalytic Applications. Results in Chemistry, 15, (2025) 102248. https://doi.org/10.1016/j.rechem.2025.102248

[18] S. Thamizharasan, K. Gurunathan, K. Varaprasad, K. Chandrasekaran, Green Engineering of MgO Nanoparticles: Assessment of their Antioxidant and Antibacterial Activity Against Dental Pathogens. Inorganic Chemistry Communications, 169, (2024) 113025. https://doi.org/10.1016/j.inoche.2024.113025

[19] R. Pugazhendhi, R. Prabhu, K. Muruganantham, R. Shanmuganathan, S. Natarajan, Anticancer, Antimicrobial and Photocatalytic Activities of

Green Synthesized Magnesium Oxide Nanoparticles (MgO NPs) using Aqueous Extract of *Sargassum Wightii* Journal of Photochemistry and Photobiology B: Biology, 190, (2019) 86–97. https://doi.org/10.1016/j.jphotobiol.2018.11.014

[20] P. Bhattacharya, A. Dey, S. Neogi, An Insight into the Mechanism of Antibacterial Activity by Magnesium Oxide Nanoparticles. Journal of Materials Chemistry B, 9(26), (2021) 5329-5339. https://doi.org/10.1039/d1tb00875g

[21] W.M. Girma, M.S. Aragie, B.A. Berehe, A.H. Aseen, Biogenic Synthesis and Characterization Of MgO Nanoparticles using Verbascum Sinaiticum: Antibacterial, Free Radical, and Reactive Oxygen Species Scavenging Activities. Materials Advances, 6, (2025) 4003–4015. https://doi.org/10.1039/d4ma01279h

[22] S.P. Singh, H. Yadav, H. Chauhan, V. Hada, K.N. Singh, Novel Approach to Enhance Antifungal Properties via Formation of Wavy and Sharp Microstructures Composed of Metal Oxide Nanoparticles and Carbon Dots. Scientific Reports, 15, (2025) 25483. https://doi.org/10.1038/s41598-025-10897-z

[23] N. Liu, F. Jiang, Z. Feng, S. Mei, Y. Cui, Y. Zheng, W. Yang, B. Wang, W. Zhang, J. Xie, N. Zhang, MgO@$SiO_2$ Nanocapsules: A Controlled Magnesium Ion Release System for Targeted Inhibition of Osteoarthritis Progression. Nanoscale Advances, 7(7), (2025) 1814–1824. https://doi.org/10.1039/d4na00900b

[24] M.I. Amrin, M.M. Roshan, R.S. Gowri, Bio-Inspired Synthesis of Magnesium Oxide Nanoparticles: Investigation of their Structural, Thermal and Optical Characteristics. Journal of Luminescence, 286, (2025) 121347. https://doi.org/10.1016/j.jlumin.2025.121347

[25] S. Mei, F. Jiang, N. Liu, Z. Feng, Y. Zheng, W. Yang, W. Zhang, Y. Cui, W. Wang, J. Xie, N. Zhang, Sol-gel Synthesis of Magnesium Oxide Nanoparticles and their Evaluation as a Therapeutic Agent for the Treatment of Osteoarthritis. Nanomedicine, 19(23), (2024) 1867–1878. https://doi.org/10.1080/17435889.2024.2382421

[26] G. Kasi, N. Stalin, P. Rachtanapun, K. Jantanasakulwong, J.N. Halder, S. Phongthai, P. Worajittiphon, J. Seo, S. Thanakkasaranee, Effect of calcination temperatures on crystallite size, particle size, and antimicrobial activity of synthesized MgO and its cytotoxicity. International Journal of Molecular Sciences, 26(10), (2025) 4868. https://doi.org/10.3390/ijms26104868

[27] Y. Saadu Itas, M.U. Khandaker, M. Mahmoud, Evaluating the CO2 capture potential of MgO sheets: a DFT study on the effects of vacancy and Ni doping for assessing environmental sustainability. RSC Advances, 15(5), (2025) 3047–3059. https://doi.org/10.1039/d4ra08592b

[28] R. Hazarika, B. Kalita, Effect of oxygen vacancy defects on electronic and optical properties of MgO monolayers: First principles study. Materials Science and Engineering: B, 286, (2022) 115974. https://doi.org/10.1016/j.mseb.2022.115974

[29] J. Tauc, (2012). Amorphous and Liquid Semiconductors. Springer Science & Business Media. https://doi.org/10.1007/978-1-4615-8705-7

[30] B.Ç. Toprak, H.İ. Efkere, S.Ş. Aydın, A. Tataroğlu, S. Özçelik, Structural, morphological, optical and electrical characterization of MgO thin films grown by sputtering technique on different substrates. Journal of Materials Science: Materials in Electronics, 35(20), (2024) 1389. https://doi.org/10.1007/s10854-024-13116-z

[31] A. Almontasser, A. Parveen, Probing the effect of Ni, Co and Fe doping concentrations on the antibacterial behaviors of MgO nanoparticles. Scientific Reports, 12(1), (2022) 7922. https://doi.org/10.1038/s41598-022-12081-z

## Authors Contribution Statement

N. Backiyalakshmi: Conceptualization, Methodology, Investigation, Data curation, Formal analysis, Writing – original draft, Visualization. S. Sindhu Kavi: Software, Validation, Resources, Formal analysis, Writing – review & editing. R. Manoranjitham: Methodology, Supervision, Project administration, Validation, Writing – review & editing. A. Ramalingam: Conceptualization, Supervision, Resources, Project administration, Writing – review & editing. All authors have read and approved the final version of the manuscript.

## Funding

The authors declare that no funds, grants or any other support were received during the preparation of this manuscript.

## Competing Interests

The authors declare that there are no conflicts of interest regarding the publication of this manuscript.

## Data Availability

The data supporting the findings of this study can be obtained from the corresponding author upon reasonable request.

## Has this article screened for similarity?

Yes

## About the License

© The Author(s) 2026. The text of this article is open access and licensed under a Creative Commons Attribution 4.0 International License.